14th International Symposium on Turbulence and Shear Flow Phenomena (TSFP14)
Heidelberg, Germany, July 28–31, 2026

OPTIMIZATION OF DISTRIBUTED JET CONTROL FOR TURBULENT FLOW SEPARATION ON A CURVED RAMP

Zhi Wu
Centre for Turbulence Control
Harbin Institute of Technology
HIT campus, Shenzhen, Guangdong, China
wuzhi@hit.edu.cn

Ge Xu
Centre for Turbulence Control
Harbin Institute of Technology
HIT campus, Shenzhen, Guangdong, China
xuge0026@gmail.com

Shengtai He
Centre for Turbulence Control
Harbin Institute of Technology, Shenzhen
HIT campus, Shenzhen, Guangdong, China
17390955857@163.com

Yu Zhou
College of Engineering
Eastern Institute of Technology, Ningbo
Ningbo, Zhejiang, China
yuzhou@hit.edu.cn

ABSTRACT

This study investigates the control of flow separation over a two-dimensional curved ramp at Reynolds number of $Re_\theta = 5700$, based on the momentum thickness of the incoming turbulent boundary layer. The control strategy employs three tangential jets issuing from spanwise slits located at three different streamwise positions on the ramp. Both steady and unsteady blowing are studied, with the objective of minimizing the recirculation region and reducing power consumption. Genetic algorithm (GA) is used to optimize the jet actuation parameters of the jets. The results show that a single steady jet positioned at the time-averaged separation point is more effective than synchronized multiple steady jets in suppressing flow separation. However, the GA-optimized steady control achieves complete elimination of the separation bubble while reducing the energy consumption by up to 30% relative to the single-jet case. The GA-optimized unsteady blowing further reduces the power consumption by 77%. The underlying flow physics associated with these control strategies are also discussed.

INTRODUCTION

In transportation vehicles such as aircraft, automobiles, and high-speed trains, turbulent flow tends to separate from the surface when subjected to a strong adverse pressure gradient. Once separation occurs, the resulting recirculation region increases aerodynamic drag and noise, thereby adversely affecting energy consumption, passenger comfort, and operational safety. To address this issue, various control strategies have been proposed, including both passive and active techniques. Passive methods, such as vortex generators, can effectively reduce the size of the recirculation region. For example, Shinde *et al.* (2016) used vortex generators to control flow separation over a backward-facing ramp and reduced the recirculation region by 20%. However, passive techniques lack flexibility and are therefore less suitable for varying operating conditions.

In contrast, active flow control is more flexible and adjustable. For example, Dandois *et al.* (2007) suppressed turbulent flow separation over a curved ramp using synthetic jets and achieved a 54% reduction in the separation bubble. He *et al.* (2023) found that a single spanwise jet, positioned near the mean separation location and operated with an appropriate velocity ratio and blowing angle, could completely suppress the separation. Other active control methods have also been applied to turbulent separation control, including spanwise alternating distributed-strip control (Ni *et al.*, 2019), sweeping jets (Koklu & Owens, 2017), jet vortex generators (Selby *et al.*, 1992), and plasma actuators (Rizzetta & Visbal, 2010). However, the associated power consumption can be prohibitively high, which has limited the widespread industrial application of these techniques.

Among the available active control approaches, unsteady blowing has attracted particular attention as a promising method for efficient separation control. In this strategy, the jets are operated in a periodic or pulsed manner rather than continuously. The advantages of unsteady blowing are twofold. First, time-dependent forcing can exploit the inherent instabilities of the separated shear layer and promote the development of large-scale coherent vortical structures, thereby enhancing momentum transfer between the outer high-momentum flow and the near-wall low-momentum region more effectively than steady blowing (Cui *et al.*, 2015; Tricouros *et al.*, 2022). Second, because the actuation is applied intermittently, the time-averaged momentum input can be significantly reduced, offering the potential for substantial energy savings (Amitay & Glezer, 2002). These features make unsteady blowing particularly attractive for turbulent separation control over curved ramps.

In the present study, three independent blowing jets are deployed on the curved ramp. Each jet can be operated in either steady or pulsed mode. To determine the globally optimal control parameters for multiple steady or unsteady jets, genetic algorithm is employed to optimize the actuation parameters with the aim of suppressing flow separation while minimizing power consumption.

EXPERIMENTAL SETUP

The experiments were performed in a closed-circuit wind tunnel with a test section of $5.5\ \mathrm{m} \times 1.0\ \mathrm{m} \times 0.8\ \mathrm{m}$ ($L \times H \times W$), featuring a flow non-uniformity of 0.1% and a longitudinal turbulence intensity of 0.4%. As illustrated in Fig. 1(a), the flow-separation-control platform, modeled after He *et al.* (2023), was mounted horizontally on the tunnel floor. It comprised a leading edge, tripping devices, an upstream flat plate, a curved ramp, and a downstream plate. The leading edge was shaped to prevent separation, while the tripping devices ensured that the boundary layer transitioned to turbulence upstream of the ramp. The curved ramp (height $h = 77.2$ mm, length $L = 202$ mm) induced flow separation due to an adverse pressure gradient. The experiments were conducted at $Re_\theta = 5700$ with a free-stream velocity of $U_\infty = 9.0$ m/s. The coordinate system is defined in Fig. 1(b), with $x = 0$ at the start of the ramp and $y = 0$ on the surface of the downstream plate. The ramp was equipped with three spanwise slits at $x/h = 0.95$, 1.50, and 1.95, each consisting of eight cavities that issued tangential jets. The compressed air was filtered, regulated, and metered before passing through the solenoid valves. The solenoid valves were driven by three independent pulsed signals to generate three pulsed blowing jets, and they remained open during steady blowing.

The three blowing jets were controlled independently. For the steady-control case, the genetic algorithm was used to optimize the blowing velocity of each jet, U_i ($i = 1,2,3$). For unsteady blowing, nine control parameters were considered: the driving pressure of each jet (P_{e1}, P_{e2}, P_{e3}), the duty cycles (DC_1, DC_2, DC_3), the phase differences between adjacent jets (φ_1, φ_2), and a common driving frequency f_e for the three jets. To suppress flow separation while minimizing power consumption, the pressure coefficient at the end of the curved ramp, $C_{p,end}$, was selected, following He *et al.* (2023), as an indicator of the separation state. The GA cost function was defined as

$$J = \left|C_{p,end} - C_{p,ref}\right| + \alpha E, \quad (1)$$

where $C_{p,ref}$ denotes the pressure coefficient at the end of the ramp when the flow is fully suppressed by a single blowing jet, E is the actuation power consumption, and α is a weighting factor that balances pressure recovery against energy expenditure. The energy term E is defined as

$$E = \frac{1}{T}\int_0^T \left[(V_{r1})^3 + (V_{r2})^3 + (V_{r3})^3\right] dt, \quad (2)$$

where the velocity ratio is given by $V_{ri} = U_i/U_\infty$ ($i = 1,2,3$). Because the jet-exit velocity is difficult to measure directly during the experiment, U_j was estimated from P_e using a predetermined polynomial model relating U_j to P_e for the steady-blowing mode. Since the performance of pulsed jets is mainly determined by the pressure amplitude (P_e), duty cycle (DC), and forcing frequency (f_e), a fully connected neural network with two hidden layers, each containing 40 nodes, was employed to predict the power consumption E from the these actuation parameters. Owing to their ability to approximate complex nonlinear relationships, neural networks are well suited for this task. Within the actuator operating range of $P_e = 0$–0.25 MPa, $DC = 0.2$–0.8, and $f_e = 20$–200 Hz, 700 parameter combinations were uniformly sampled and used to drive the jet. The corresponding outlet velocity was measured using a hot-wire anemometer, and the power consumption was calculated according to Eq. 2. These 700 data samples were used to train the neural network.

GA-OPTIMIZED STEADY FORCING

As discussed earlier, the weight α in the cost function, which balances the two objectives, is crucial for optimization. A larger α causes the optimization to prioritize reducing energy consumption, whereas a smaller α places greater emphasis on pressure recovery. The optimization was performed for different values of α. The minimum cost J_1^n in each generation gradually decreases as the generation number n increases, eventually converging to 0.137, 0.097, and 0.038 for α = 0.47, 0.28, and 0.09, respectively (Fig.2a). At α = 0.09, $\mid C_{p,end} - C_{p,ref} \mid$ and E converge to 0.001 and 0.397, respectively, after 16 generations, indicating successful suppression of flow separation. This result confirms that α = 0.09 is an effective choice for suppressing flow separation.

The convergence histories of the control variables V_{r1}, V_{r2}, and V_{r3} for $\alpha = 0.09$ are presented in Fig. 2b, from which several noteworthy observations can be made. First, V_{r1} converges to zero, indicating that the blowing jet located at $x/h = 0.95$ does not contribute positively to flow-separation suppression. Second, among the three control variables, the converged value of V_{r2} is consistently the largest, following the general trend

$$V_{r2} > V_{r3} > V_{r1} = 0.$$

This result suggests that the blowing jet at $x/h = 1.50$, which is positioned slightly upstream of the mean separation location, plays the dominant role in suppressing flow separation. This observation is in good agreement with our previous conventional control results, which showed that tangential blowing applied slightly upstream of the separation point is more effective than blowing at other locations. A similar conclusion was also reported by He *et al.* (2023).

Figure 3 compares the control efficiency of single-jet and GA-optimized multiple steady blowing based on the energy consumption ratio (E/E_{ref}) and the pressure recovery ratio ($C_{p,end}/C_{p,ref}$). The steady single-jet blowing located at the mean separation point, operated at $U_2 = 0.82U_\infty$, was chosen as a benchmark due to its proven effectiveness among steady single-jet configurations. The results demonstrate a trade-off between energy consumption and pressure recovery achievable through GA optimization. For instance, at α = 0.09, the GA-optimized control attains the same pressure recovery as the reference case while consuming 30% less energy, effectively eliminating the recirculation region. At α = 0.28, it achieves 86% of the reference pressure recovery with a 54% reduction in energy input. This trend remains consistent even with slight variations in the reference case.

GA-OPTIMIZED UNSTEADY FORCING

In the unsteady-control mode, GA was used to optimize the nine control parameters. For α=0.25, the J_1^n, J_p and E eventually converged to 0.032, 0 and 0.0046, respectively. Figure 4 shows the learning curves of the best control parameters in each generation. It is noteworthy that the optimized driving

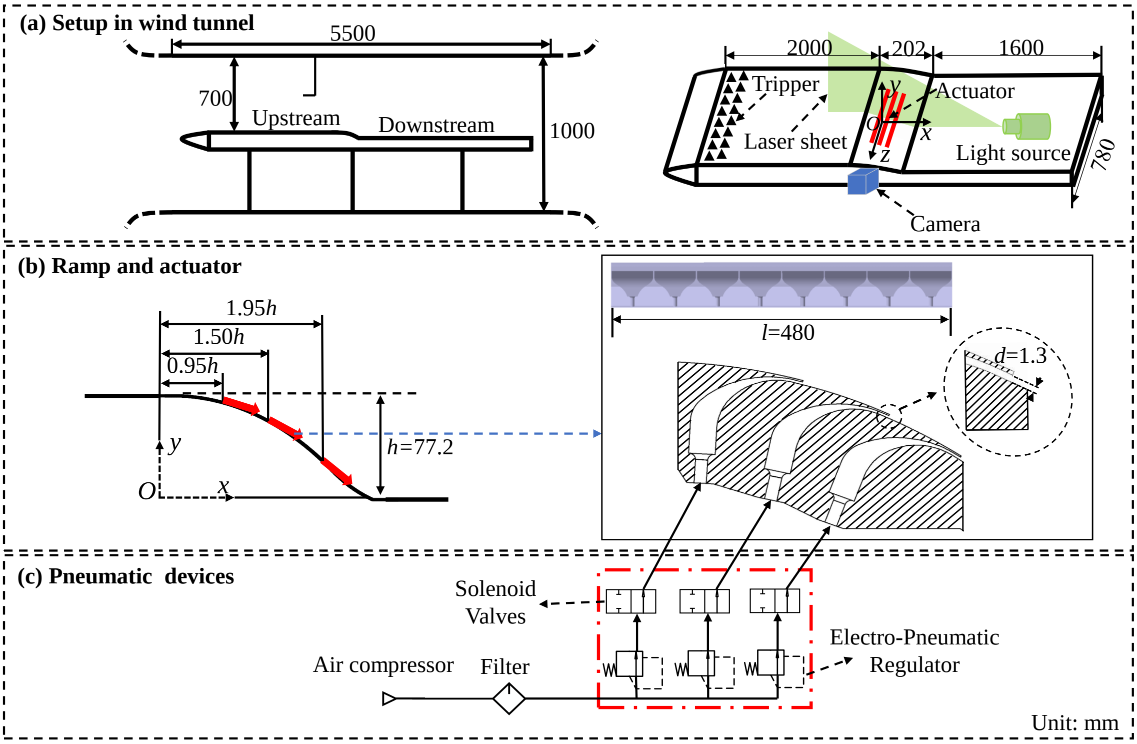

Figure 1. Experimental setup and actuation system. (a) Experimental model of the upstream and downstream flat plates and the curved ramp; (b) design of the actuation system on the ramp.

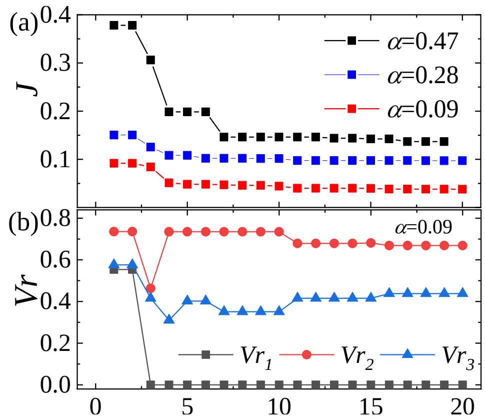

Figure 2. Learning curves of (a) cost function J and (b) control parameters V_{r1}, V_{r2} and V_{r3} at $\alpha = 0.09$.

pressure P_{e2}, corresponding to the jet located at $x/h = 1.50$, is higher than both P_{e1} and P_{e3} (see Fig.4a). This result indicates that jet 2 plays the most important role in separation control, which is consistent with the trend observed in the steady blowing case. In addition, the optimized duty cycles (DC) of all three jets converge to a narrow range of 0.20–0.24 (see Fig.4b), while the forcing frequency f_e approaches approximately 106 Hz (see Fig.4d). It should be emphasized that $DC = 0.20$ represents the lower bound of the prescribed search range. Under the optimized condition of $DC = 0.20$ and $f_e = 106$ Hz, the corresponding pulse width is 1.89 ms, which is already close to the hardware limit of 1.2 ms. Any further reduction in pulse width may induce a choked-flow effect and is therefore not practically feasible.

The control efficiency of a single steady jet and GA-optimized unsteady jet is compared in Fig. 3 using E/E_{ref} and

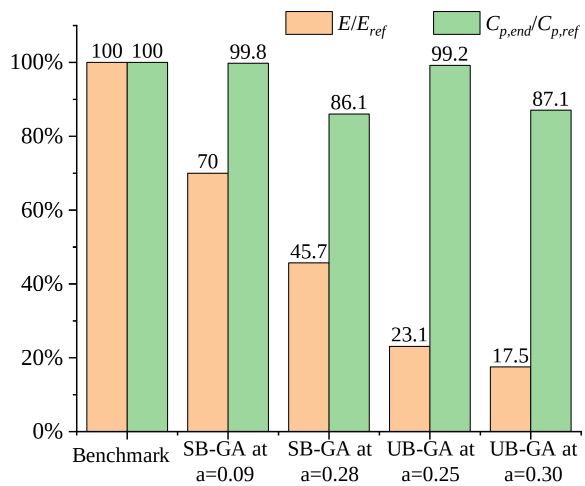

Figure 3. The pressure recovery rate and the corresponding power consumption rate under different control configurations: the optimal steady blowing using one jet (Benchmark), GA-optimized steady blowing (SB-GA) and unsteady blowing (UB-GA) under different α.

$C_{p,end}/C_{p,ref}$. The results demonstrate that the GA-optimized unsteady blowing achieves significantly higher energy savings than the benchmark case. At $\alpha = 0.25$, it attains nearly the same pressure recovery as the benchmark case with only 23.1% of the energy consumption—a 76.9% reduction—while completely suppressing the recirculation region. At $\alpha = 0.30$, it maintains 85.8% of the pressure recovery with just 17.5% of the reference energy. As α increases, the optimization prioritizes lower energy input, which consequently leads to diminished pressure recovery. Furthermore, the GA-optimized unsteady control is more efficient than the GA-optimized steady

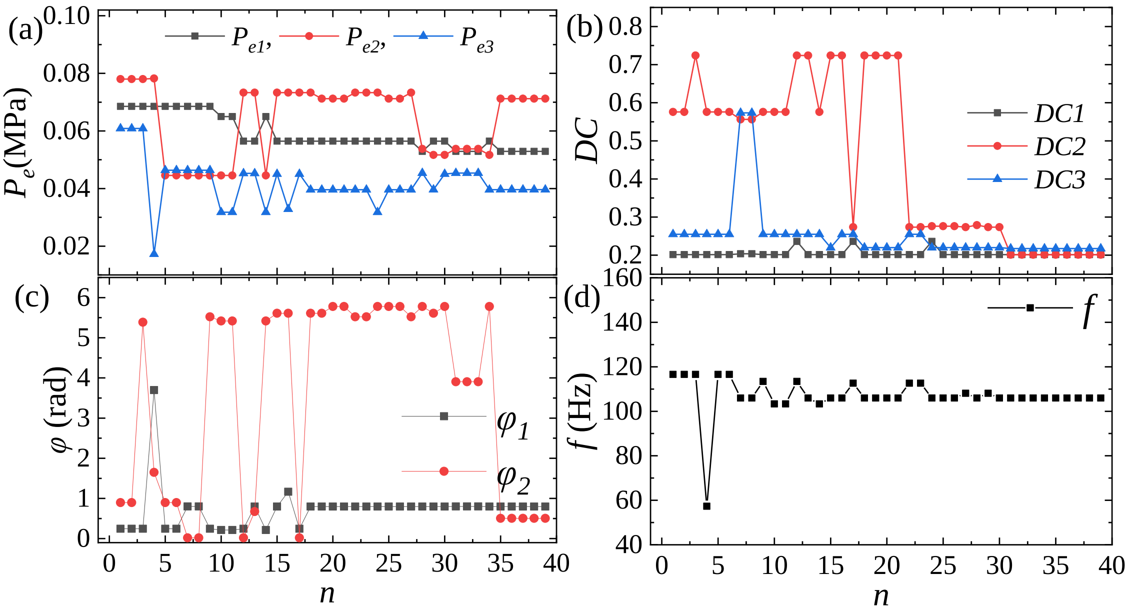

Figure 4. Learning curves of (a) P_e, (b) DC, (c) φ and (d) f_e for GA control at $\alpha = 0.25$.

control, showing greater potential for industrial applications.

FLOW FIELD ANALYSIS

Figure 5 shows the time-averaged streamlines and contours of U/U_∞ under different control configurations. Figure 5(a) presents the baseline uncontrolled case, where flow separation occurs downstream of $x/h \approx 1.5$, forming a large recirculation bubble that does not reattach until $x/h \approx 3.8$. This separation is completely suppressed in the reference case (Fig. 5b) via steady single-jet blowing at $x/h = 1.50$. The flow field of the GA-optimized steady forcing at $\alpha = 0.09$ (Fig. 5c) is almost identical to that of the reference case. This observation, which agrees well with the pressure measurements in Fig. 3, indicates that the flow separation is fully suppressed. The flow field for the GA-optimized unsteady forcing at $\alpha = 0.25$ (Fig. 5d) exhibits minimal flow separation, with the flow remaining attached downstream despite some residual disturbances. The comparable pressure recovery to the reference case and GA-optimized steady blowing at $\alpha = 0.09$ (Fig. 3) confirms a similar control effectiveness. In contrast, for α = 0.30 (not shown), a discernible recirculation region persists, indicating reduced control effectiveness. This is consistent with the optimization objective at a higher α value, which prioritizes energy saving over pressure recovery, leading to lower actuation energy and consequently weaker flow control. Overall, the GA-optimized strategy effectively suppresses flow separation under all the tested conditions.

Because the GA-optimized unsteady control exhibits higher control efficiency than the steady control, a key question is why the optimal actuation occurs at $f_e = 106$ Hz with a phase difference of about $0.1T$, and what physical mechanism governs this result. Figure 6 shows the phase-averaged streamlines and Q-criterion contours for $\alpha = 0.25$ at different actuation phases. Owing to the interaction between the pulsed jet and the main flow, a spanwise vortex is generated at the leading edge of each jet pulse, marked by the red dots in Fig. 6. Within one actuation cycle, the vortex generated by slit S_1 convects downstream and reaches the location of slit S_2, where it merges with the vortex produced by the subsequent pulse from S_2. Therefore, the apparent phase lead of $0.1T$ is physically equivalent to a lead of $1.1T$ across successive cycles. At $f_e = 106$ Hz, corresponding to a period of 9.5 ms, this timing allows the vortex generated by S_1 to arrive at S_2 in synchrony with the next pulse from S_2, thereby promoting vortex merging and enhancing control effectiveness. This also suggests that the optimal frequency and phase difference depend on the spacing between the two slits.

CONCLUSION
Conclusion

In this study, three independently controlled blowing jets were arranged on a curved ramp to suppress turbulent flow separation. A genetic-algorithm-based optimization was performed for both steady and unsteady blowing cases, with the dual objective of minimizing the recirculation region and reducing control power consumption. The main conclusions are summarized as follows.

1. GA-optimized steady blowing can effectively suppress the separated flow while reducing energy consumption. The optimal steady control completely removes the recirculation region, achieving a control effect comparable to that of the optimal single-jet steady blowing, but with a 30% reduction in energy consumption. For both steady and unsteady blowing, the jet located near the mean separation point is the most effective. In the steady case, the control effectiveness decreases rapidly when the jet is moved upstream. The energy saving of the optimal steady control is mainly achieved by reducing the maximum blowing intensity near the separation point and introducing an additional low-speed jet downstream, which helps accelerate the local near-wall flow and suppress the residual separation more efficiently.
2. GA-optimized unsteady blowing is significantly more efficient than the optimized steady blowing. It can almost completely eliminate the recirculation region while requiring only 23.1% of the energy consumption of the optimal single steady blowing case. The superior performance of the unsteady strategy is attributed to spatiotem-

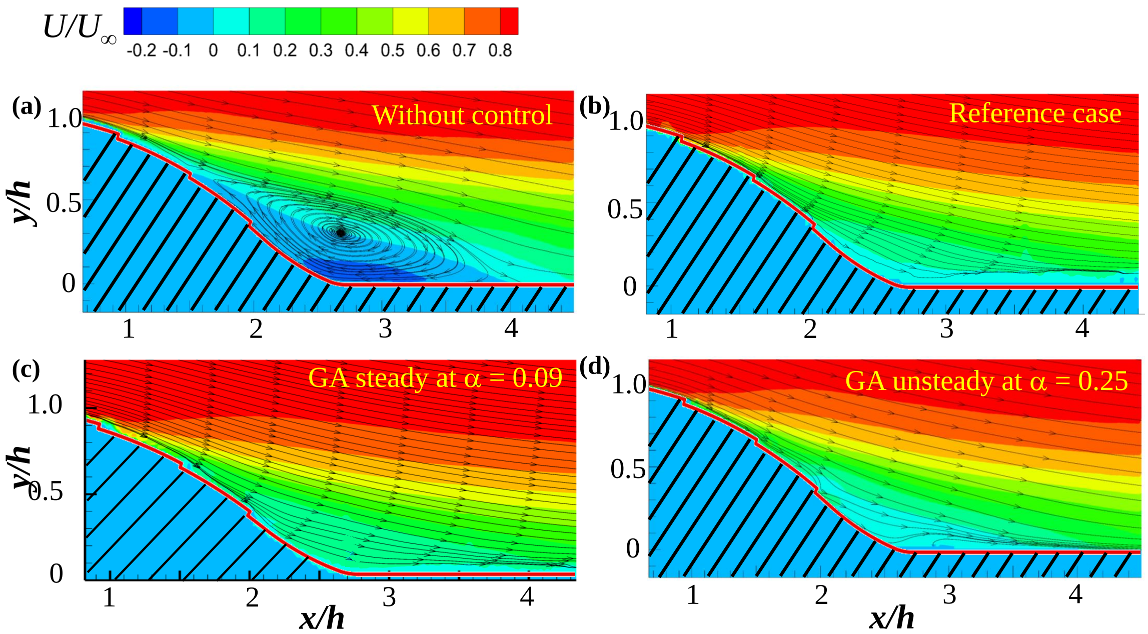

Figure 5. Time-averaged streamlines and contours of U/U_∞ under different control modes (a) without control; (b) single steady jet at $V_r = 0.82$; GA-optimized blowing at (c) $\alpha = 0.25$ and (d) $\alpha = 0.30$.

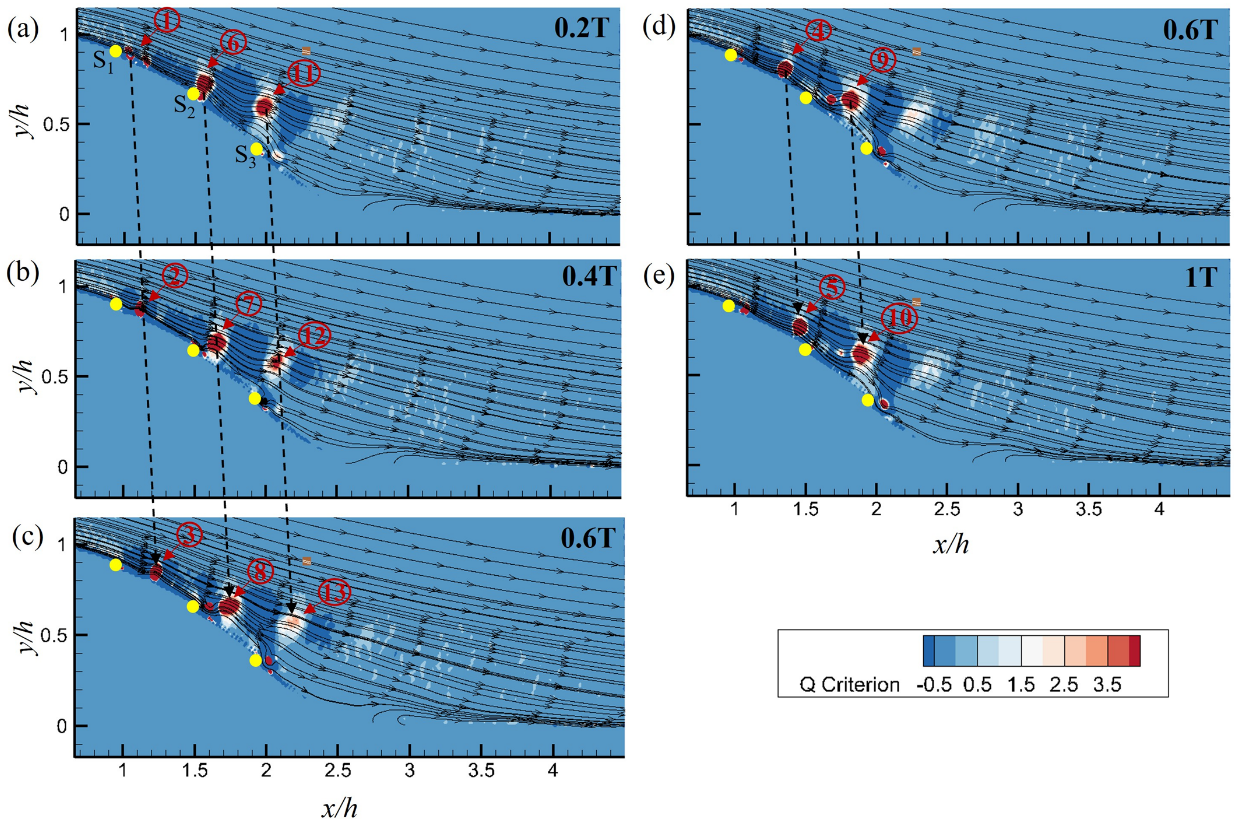

Figure 6. Phase-averaged streamlines superimposed on phase-averaged contours of the Q-criterion for $\alpha = 0.25$ at different phases: $0.2T$, $0.4T$, $0.6T$, $0.8T$ and T. The yellow dots denote the slit positions. $T = 1/f_e$

porally coordinated actuation among the jets. The pulsed blowing generates two favorable effects: a Coandă effect immediately downstream of the jet exit and spanwise vortices developing near the ramp surface. The former induces a low-pressure region near the wall and promotes strong downwash motion, whereas the latter enhances momentum transport within the boundary layer. In particular, the actuation of Jet 1 strengthens the effect of Jet 2, leading to a stronger Coandă effect and more pronounced spanwise vortices. The combined action of these mechanisms is responsible for the highly efficient suppression of flow separation.

ACKNOWLEDGMENT

The authors wish to acknowledge supports from the Research Grants Council of the Shenzhen Government (Grant No. GXWD20220811152110003), NSFC (Grants No. 12202123 and U24B2005), and the Aeronautical Science Foundation of China (Grant No. 2024M033077002).

REFERENCES

Amitay, Michael & Glezer, Ari 2002 Controlled transients of flow reattachment over stalled airfoils. *International Journal of Heat and Fluid Flow* **23** (5), 690–699.

Cui, Wenshi, Zhu, Hui, Xia, Chao & Yang, Zhigang 2015 Comparison of steady blowing and synthetic jets for aerodynamic drag reduction of a simplified vehicle. *Procedia Engineering* **126**, 388–392, frontiers in Fluid Mechanics Research.

Dandois, Julien, Garnier, Eric & Sagaut, Pierre 2007 Numerical simulation of active separation control by a synthetic jet. *Journal of Fluid Mechanics* **574**, 25–58.

He, Shengtai, Zhang, Kai, Song, Yukuan & Zhou, Yu 2023 Control of flow separation from a curved ramp using a steady-blowing jet. *Physics of Fluids* **35** (4), 045139.

Koklu, Mehti & Owens, Lewis R. 2017 Comparison of sweeping jet actuators with different flow-control techniques for flow-separation control. *AIAA Journal* **55** (3), 848–860.

Ni, Weidan, Lu, Lipeng, Fang, Jian, Moulinec, Charles, Emerson, David R. & Yao, Yufeng 2019 Flow separation control over a rounded ramp with spanwise alternating wall actuation. *Physics of Fluids* **31** (1), 015101.

Rizzetta, Donald P. & Visbal, Miguel R. 2010 Large-eddy simulation of plasma-based turbulent boundary-layer separation control. *AIAA JOURNAL* **48** (12), 2793–2810, 39th AIAA Fluid Dynamics Conference and Exhibit, San Antonio, TX, JUN 22-25, 2009.

Selby, GV, Lin, JC & Howard, FG 1992 Control of low-speed turbulent separated flow using jet vortex generators. *EXPERIMENTS IN FLUIDS* **12** (6), 394–400.

Shinde, Siddhesh, Tandon, Suyash, Maki, Kevin & Johnsen, Eric 2016 Flow separation over a backward-facing ramp with and without a vortex generator. In *46th AIAA Fluid Dynamics Conference*, p. 3795.

Tricouros, Frank A., Amitay, Michael & Van Buren, Tyler 2022 Comparing steady and unsteady rectangular jets issuing into a crossflow. *Journal of Fluid Mechanics* **942**, A56.